Title

Uncovered Dynamic Coupling Resolves the Ambiguous Mechanism of Phenylalanine Hydroxylase Oxygen Binding

Journal

The Journal of Physical Chemistry B, 123(21)

ISSN

1520-6106

Authors

Reilley, David J
Popov, Konstantin I
Dokholyan, Nikolay V
et al.

Publication Date

2019-05-30

DOI

10.1021/acs.jpcb.9b02893

Peer reviewed

Uncovered Dynamic Coupling Resolves the Ambiguous Mechanism of Phenylalanine Hydroxylase Oxygen Binding

David J. Reilley,[†] Konstantin Popov,[‡] Nikolay V. Dokholyan,[¶,‡] and Anastassia N. Alexandrova[*,†,§]

[†]*Department of Chemistry and Biochemistry, University of California, Los Angeles, 410 Westwood Plaza, Los Angeles, CA 90095, USA*

[‡]*Department of Biochemistry and Biophysics, University of North Carolina at Chapel Hill, Chapel Hill, NC 27599, USA*

[¶]*Department of Pharmacology, Department of Biochemistry & Molecular Biology, Penn State University College of Medicine, Hershey, PA 17033, USA*

[§]*California NanoSystems Institute, University of California, Los Angeles, 570 Westwood Plaza, Los Angeles, California 90095-1569, USA*

E-mail: ana@chem.ucla.edu

Phone: +1 310 8253769

Abstract

Phenylalanine hydroxylase (PAH) is an iron enzyme catalyzing the oxidation of L-Phe to L-Tyr during phenylalanine catabolism. Dysfunction of PAH leads to the debilitating condition phenylketonuria (PKU), which prompted research into the structure and function of PAH over the last 50 years. Despite intensive study, there is no consensus on the atomistic details of the mechanism of O_2 binding and splitting by wild type PAH and how it varies with PKU-inducing mutations, Arg158Gln and Glu280Lys. We studied structures involved in a proposed mechanism for the wild type and mutants using extensive mixed quantum-classical molecular dynamics simulations. Simulations reveal a previously unobserved dynamic coupling between active site and the mutation sites, suggesting how they can affect the catalytic performance of PAH. Furthermore, the effect of the coupling on PAH structure agrees with and expands our understanding of the experimentally observed differences in activity between the wild type and mutants.

Introduction

While phenylalanine hydroxylase (PAH) is critically implicated in a range of problems of medical and biological interest, its activity is not fully understood. It is an important metabolic protein responsible for phenylalanine catabolism[1–3] and over 280 different mutants of the protein have been genetically linked to the well-studied condition phenylketonuria (PKU),[4] a candidate for gene therapy.[5] Two mutants of particular interest are R158Q, which is a common mutant as it comprises 40% of PKU haplotype 4 alleles in Europe,[6] and E280K, which is unusual among PKU mutants as it found on multiple haplotypes.[7] The protein is highly similar to both tryptophan hydroxylase and tyrosine hydroxylase, which perform the same function on their respective amino acids.[1] PAH is found as a highly conserved homodimer or homotetramer of 51.7 kDa subunits,[8,9] with an iron center in each monomeric unit that binds and cleaves diatomic oxygen.[10,11] Activated oxygen then participates in one

of two competing pathways: the oxidation of phenylalanine to tyrosine, which dominates in wild type PAH, or the formation of hydrogen peroxide, which dominates in the PKU-inducing mutants.[12] Despite all the interest in PAH, two critical features in this mechanism of O_2 binding and activation are poorly understood. First, both PKU-inducing mutantions, Arg158Gln and Glu280Lys, occur far from the active site. X-ray crystallography shows that in the wild type these two residues form a salt bridge around 20 Å away from the iron center (Figure 1). Why the disruption of this distant interaction affects PAH activity has not been firmly established. The second is the role of a (6R)-L-erythro-5,6,7,8-tetrahydrobiopterin (BH_4) cofactor. The binding of BH_4 to the active site is necessary for PAH function, where it presumably assists the iron center in binding and cleaving O_2. Despite extensive study, including on tryptophan hydroxylase and tyrosine hydroxylase which suggest they operate by the same general pathway,[13–16] no research to date fully resolves either of these specific questions.

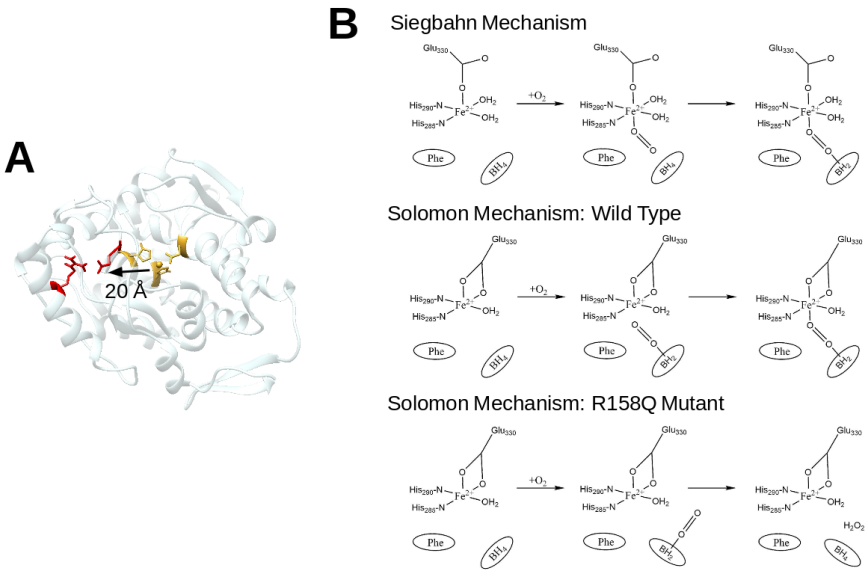

Figure 1: (A) The phenylketonuria inducing mutants (red) of phenylalanine hydroxylase (PAH) are surprisingly far from its active site (yellow). (B) The oxygen activating and cleaving activity of PAH is not well understood structurally. In the Siegbahn mechanism, the metal has an additional water ligand and oxygen binds to the metal before the cofactor. According to the Solomon mechanism a change in orientation of the cofactor could explain the preferential H_2O_2 forming activity of the mutant.

Our study starts with structures implicated in a prominent mechanism put forward by the laboratory of Prof. Solomon based on spectroscopic data,[12] which posits solid initial hypotheses on our two mechanistic questions but lacks sufficient atomistic evidence to support them. This mechanism hypothesizes that O_2 binds first to BH_4 and then to the metal in the natural, tyrosine forming pathway. It then conjectures that the cofactor is positioned improperly in the active site of the mutants, so that O_2 instead binds just to BH_4 and forms H_2O_2 in the pathological pathway. The Solomon study also notes the proximity of Arg158 to two loops around the active site identified in a previous study: one comprising residues 131-155 and another comprising residues 247-251 which forms some hydrogen-bonding contacts with the cofactor.[9,12] However, neither of these contacts fully explain the coupling between the mutant residues and the cofactor for a number of reasons. First, they hinge just on the simple proximity of Arg158 rather than specific interactions. Second, they are based on a single crystal structure of the PAH wild type and contain no information about the mutant state. Finally, as they are based on a single structure they consequentially ignore any dynamic aspects of long-range coupling. These gaps in knowledge necessitate an all-atom investigation of PAH O_2 binding activity.

We also consider structures from a potentially problematic mechanism suggested by the laboratory of Prof. Seigbahn based on DFT studies of small models of the PAH active site.[17] For the O_2 binding step of interest to us the model this mechanism utilized lacks the necessary presence of the phenylalanine substrate and has an inappropriate additional water ligand bound to the iron center rendering it inconsistent with previous kinetic and spectroscopic findings.[12] It thus corresponds more closely to an inactive form of PAH. Our consideration of this mechanism therefore acts as a negative control to see if any dynamic behavior we identify is truly unique to the O_2 binding step or a general property of the protein.

In this study, we performed extensive mixed quantum-classical dynamics simulations on the whole protein and its two pathogenic mutants at full atomistic resolution with QM/DMD,

a rapid sampling method for metalloproteins (described fully in the methods section). The active sites are specified by both the Solomon and Seigbahn mechanisms with appropriate modifications. Simulations capture the wild type (WT), R158Q, and E280K variants for the Seigbahn structures and the WT and R158Q variant for the Solomon structures, with the E280K variant excluded as its different metal coordination precludes direct comparison of energy with the wild type. Our simulations of the Seigbahn construction show it to be highly rigid, in contrast to the flexibility of the Solomon system; the difference demonstrates that the dynamic behaviors of the Solomon system are inherent to the O_2 binding step. These behaviors consist of a significant difference in cofactor orientational preference between the native and mutant forms of the protein and a robust coupling between the cofactor and mutant residues distinct from the static hydrogen-bonding networks suggested by Solomon. The obtained structural data corroborate and expand both Solomon hypotheses with necessary atomistic detail.

Theoretical Methods

A total of 7 replicates for each of the Siegbahn systems and 10 replicates for each of the Solomon systems were run. Simulations were run for 40 to 80 ns. Details about the preparation of each system and the results of the undiscussed systems can be found in the supplementary information.

The established QM/DMD method was used for these simulations.[18] This is a technique for sampling metalloprotein conformations which uses discrete molecular dynamics (DMD)[19] to describe the protein and quantum mechanical (QM) electronic structure calculations necessary to model the metal and its environs. Both methods treat an overlapping region, consisting of species participating in important, non-covalent interactions near the metal, to mitigate discontinuity errors. QM/DMD has a strong record and our group has used it to successfully explain a range of metalloenzyme behavior. These include metal-

dependent catalytic activity,[20–23] protein metal affinity,[20] sequence and cofactor-dependent redox functionality,[18,24] the role of protein electrostatics in activity,[25] effect of mutagenesis on structure,[18,26] and flexible docking to metalloenzymes.[27]

All QM calculations in this study were performed at the DFT level of theory with Turbomole (version 6.6).[28] The pure meta-GGA TPSS functional[29] with the D3 dispersion correction[30] was used. The metal was treated with the triple-zeta basis set def2-TZVPP and all other atoms with the double-zeta def2-SVP basis set.[31] While the small basis set may result in some degree of basis set superposition error, the large size of our QM regions have precluded the use of larger basis sets. Furthermore, the level of theory employed without correction has proven effective in our cited past studies including for quantitative free energy comparisons. Finally, the Conductor-like Screen Model (COSMO) with a constant dielectric of 4 was applied to approximate the screening and solvation effects in the relatively buried active sites of the systems.[32] All DMD simulations in this study were performed for 10,000 steps per iteration (0.5 ns).

Convergence of the QM/DMD simulations was achieved according to a series of metrics. These consist of the full protein all-atom RMSD (calculated with respect to all atoms in our models), active site all-atom RMSD (calculated for just the atoms in our QM region) and the DMD energy and QM energy. The RMSD values were calculated with the initial protein equilibrated for one QM/DMD iteration as the reference structure. The full protein all-atom RMSD trajectories of each system are included in this text as an example (Figure 2), while plots of the other three standards can be found in the supporting information.

Results and Discussion

The QM/DMD simulations show the Seigbahn system to be conformationally stiff, with little difference between the wild type and mutant structures. The full protein RMSDs of the PAH variants indicate well converged trajectories: 1.89 $\pm$ 0.19 Å for the WT versus

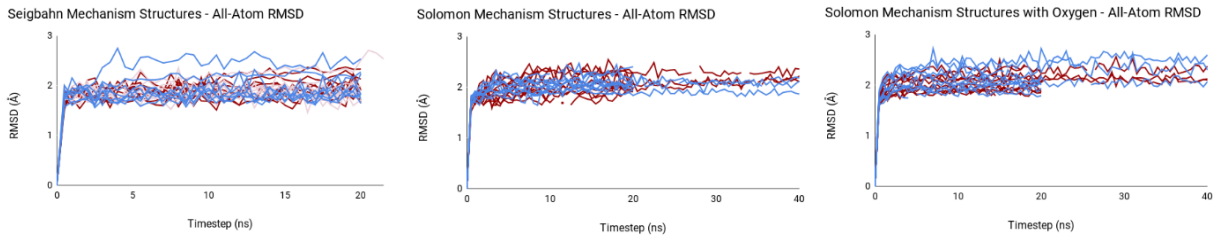

Figure 2: Plots of the full protein, all-atom RMSD by timestep for every QM/DMD simulation in this study. The plots include all replicates of the wild type (dark red), R158Q mutant (medium blue), and E280K mutant (light violet, only in Seigbahn simulations). Notice how all replicates oscillate around the value of 2 Å indicating convergence.

1.93 ± 0.26 Å for R158Q and 1.89 ± 0.19 Å for E280K. There are no significant differences between the structures of the active site, with RMSDs of 0.70 ± 0.23 Å for the WT versus 0.70 ± 0.24 Å for R158Q and 0.69 ± 0.27 Å for E280K (Figure 3). The average distances between the Fe center and the central (average) point of BH_4 are all nearly the same: 4.64 ± 0.10 Å for the WT versus 4.72 ± 0.17 Å for R158Q and 4.66 ± 0.09 Å for E280K. Even the orientation of the cofactor relative to the metal does not change with the mutations. The angle between the metal and BH_4 is 48.4 ± 2.1° for the WT versus 46.9 ± 5.5° for R158Q and 47.8 ± 1.6° for E280K. Furthermore, given the low standard deviations of these values, there are no significant populations of other angles that might characterize the position of BH_4 during the competing, H_2O_2 forming pathway. As the Seigbahn structures correspond to an inactive form of PAH, the lack of dynamic behavior in our simulations of them suggests that the behavior found for the Solomon systems is not inherent to PAH overall, but specific to its active form.

The results for the Solomon system with O_2 absent are consistent with the Solomon postulation of the role of the BH_4 cofactor. As before, the full RMSD indicates well-converged stable structures at 2.04 ± 0.20 Å for the WT versus 2.02 ± 0.14 Å for R158Q. The active site all-atom RMSD reports some difference between the WT at 1.13 ± 0.42 Å and the R158Q mutant at 1.19 ± 0.25 Å. The most important difference between the wild type and mutant here, clearly visible in Figure 3, is the metal to cofactor angles at 55.0 ± 24.3 degrees and 86.8 ± 17.3 degrees respectively. A histogram shows that the wild type has a much larger

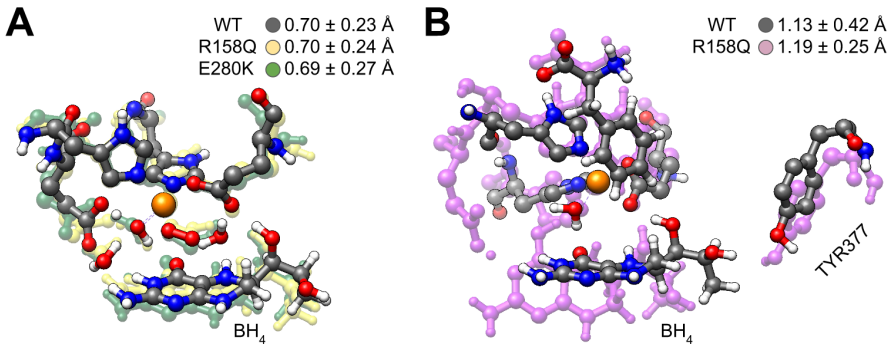

Figure 3: Equilibrated active site geometries for different forms of PAH, with reported all-atom RMSDs in the top right. (A) The wild type and mutants from the Siegbahn simulations show no significant differences in their geometries, matching their similar RMSD values. (B) On the other hand, the geometries from the Solomon mechanism without O_2 demonstrate the distinct angular preferences of BH_4. This pterin-like cofactor is angled further away from the metal center in the mutant relative to the wild type.

preference for the lower angle while the mutant greatly prefers the higher angle facing away from the metal (Figure 4). Furthermore, both angles are energetically accessible, as the average QM energy across both forms of the protein for the three most populated histogram bins of the lower angle peak is just 1.26 kcal/mol less than those of higher angle peak. Given the difference in activity between the wild type and mutant, these data suggests that the peaks about the lower and higher angles correspond to the natural and H_2O_2 forming pathways respectively. This supports the Solomon hypothesis that the orientation of the cofactor dictates PAH activity as the active site in the wild type is structurally predisposed to both BH_4 and the metal binding O_2, but the active site in the mutant is not (further supported by simulations with O_2 present in the supporting information). Furthermore, just like both variants can still perform their unpreferred pathway they each report a small fraction of the unpreferred angle.

The QM/DMD simulations of the Solomon structures also explain how the distant mutation affects such a change in active site structure and dynamics. They identify a previously unknown chain of tightly dynamically coupled residues connecting the mutant residues and the cofactor that controls its orientation. The position of BH_4 in the wild type is partially coupled to the position of the Tyr377 residue which frequently forms a hydrogen bond to

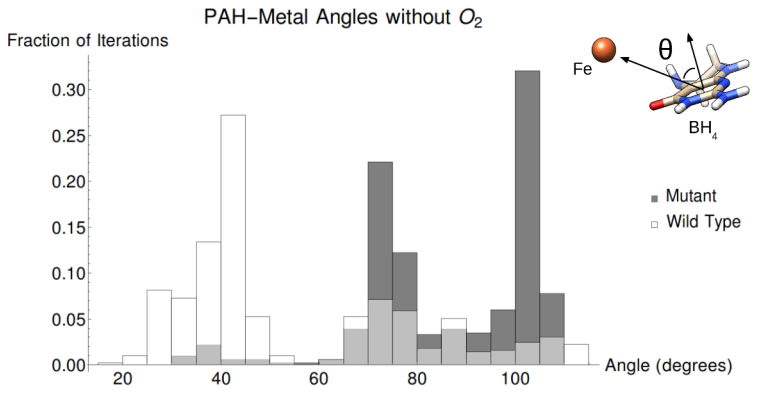

Figure 4: Histogram of the metal to cofactor angle in the Solomon mechanism system with O_2 absent for the wild type (white) and the R158Q mutant (dark gray). The height of each bar represents the percentage of iterations across all replicates with an angle in that five degree threshold. The color visible above a bar with the blended medium gray represents the form of the protein in excess for that threshold. Notice that the wild type and mutant overwhelmingly select different angles, consistent with the two pathways reported experimentally.

it. The distances between the Tyr377 phenolic oxygen or hydrogen and potential hydrogen bonding partners on BH_4 were calculated and the minimum distance selected for each iteration of all replicates for both the wild type and mutant. A histogram of this data shows that in the wild type Tyr377 typically forms a hydrogen bond to the cofactor, with a maximum of population of this length around the characteristic distance of 2.5 Å. In contrast, the mutant generally does not form this H-bond, with a maximum of population ca. 6 Å (Figure 5). Furthermore, the position of Tyr377 is tethered to the residue 158 through a series of flexible loops. This suggests that the breaking of the residue 158 to 280 salt bridge by mutation communicates directly with the position of Tyr377 and affects its interaction with BH_4. This is not a large conformational change, and so does not significantly increase the all-atom RMSD. The results indicate that in the wild type the Tyr377 residue holds the cofactor in place to control proper activity, while the mutation breaks this interaction giving BH_4 greater orientational flexibility with respect to the metal center. This then results in the prominence of the H_2O_2 forming pathway.

Additional confirmation for the discovered dynamic coupling was found through a dedicated coupled-dynamics method developed by the Dokholyan group. The method calculates

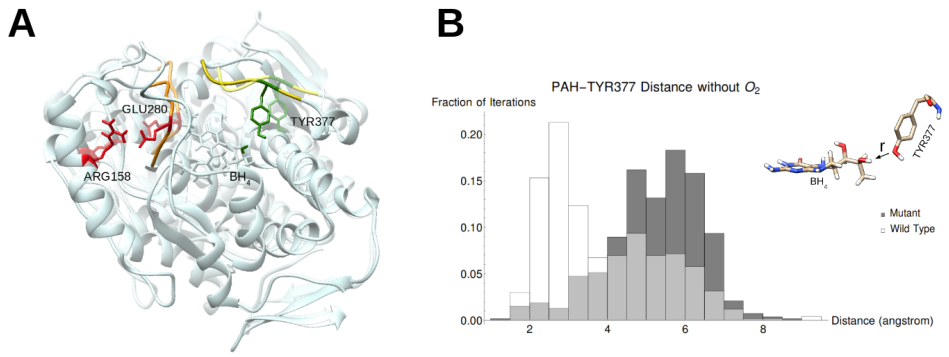

Figure 5: (A) Picture which illustrates the structural connection between the site of mutation and the active site in PAH with WT overlay on a faint R158Q structure. The mutation of one of the red residues breaks a salt bridge which in turn makes the orange loop (residues 276-281) more flexible. The orange loop then pushes the yellow loop (residues 376-381) out of its wild type position, affecting the cofactor and active site through Tyr377 (green). (B) Histogram of the BH_4 to Tyr377 minimum distance for the wild type (white) and the R158Q mutant (dark gray). The height of each bar represents the percentage of iterations across all replicates with an angle in that 0.5 Å threshold. The color visible above a bar with the blended medium gray represents the form of the protein in excess for that threshold. This chart shows that the frequency of a hydrogen-bonding interaction between these two species, which occurs around 2 to 4 angstroms, is much higher in the wild type.

correlated motions between residues and constructs pathways with Dijkstra's algorithm. It was used to great effect to study allosteric behavior in pathogenic cystic fibrosis regulator ion channel mutants.[33,34] A simplified protocol was applied to the lowest energy structure of each of the studied systems (results for the Siegbahn structures can be found in the supporting information). In the Solomon wild type, the method finds a strong coupled-dynamics pathway which connects the site of mutation to Tyr377 through the same series of loops identified in QM/DMD simulations (Figure 6). This coupled-dynamics pathway is diverted in the R158Q mutant, consistent with its looser control of the position of Tyr377.

The identified coupling between the cofactor, Tyr377, is an unique, directing interaction necessary to understand the BH_4 orientational preferences. The cofactor forms other hydrogen-bonding contacts, namely with the loop of residues 147-151. These are the most obvious interactions, as they are present in the original crystal structure (PDB: 1KW0) while the hydroxyl oxygen of the cofactor and Tyr377 are 6.39 Å apart. However, the contacts

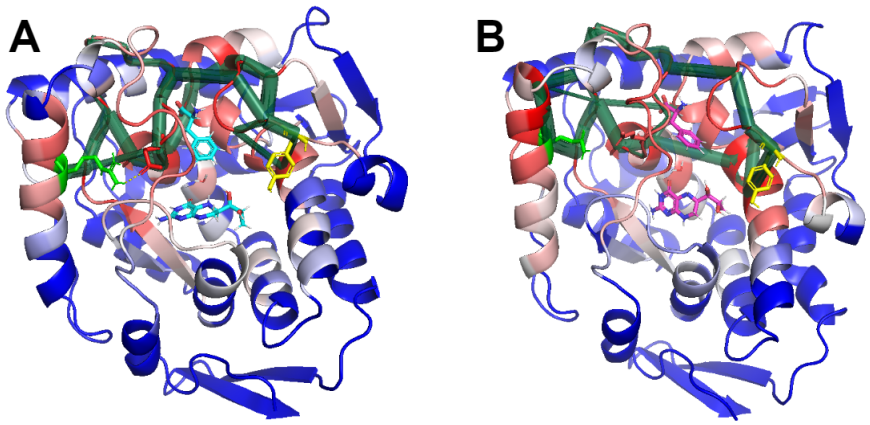

Figure 6: Coupled-dynamics pathways (deep green bars) between the site of mutation (bright green and red) and Tyr377 (yellow) identified by coupled-dynamics in the exemplary structures from QM/DMD for the Solomon system WT (A) and R158Q mutant (B). Residues are colored in a heat map going from red to blue indicating motion more to less correlated with the site of mutation. Notice how the pathways in the WT closely match the pathway identified with QM/DMD depicted in Figure 4, while those in the mutant do not.

on the 147-151 loop can't explain the cofactor angle as they change little between the wild type and mutant. On this loop, the Ser151 side chain alcohol and the Gly130 and Leu132 backbone carbonyls all form hydrogen bonds with the cofactor (Figure 7). As with Tyr377, we measured the distance between the atoms in these groups that can hydrogen bond and their nearest partner on the cofactor for all iterations of our simulations. Unlike Tyr377, the average distance of each of these contacts varies little between the wild type and mutant, at just 3.12 ± 1.48 Å (WT) vs 2.79 ± 1.10 Å (R158Q) for Ser151, 3.24 ± 1.09 Å (WT) vs 3.65 ± 1.26 Å (R158Q) for Leu132, and 3.26 ± 1.09 Å (WT) vs 2.79 ± 1.10 Å (R158Q) for Gly130, compared to a significant 3.87 ± 1.48 Å (WT) vs 5.23 ± 1.23 Å (R158Q) for Tyr377. These differences suggest that the angular preferences of the cofactor correlate with its interaction with Tyr377, but not with the nearly constant hydrogen-bonds between BH_4 and the 147-151 loop. Ultimately, it is the subtle, shifting interaction that proves most important in understanding PAH activity at an atomic level.

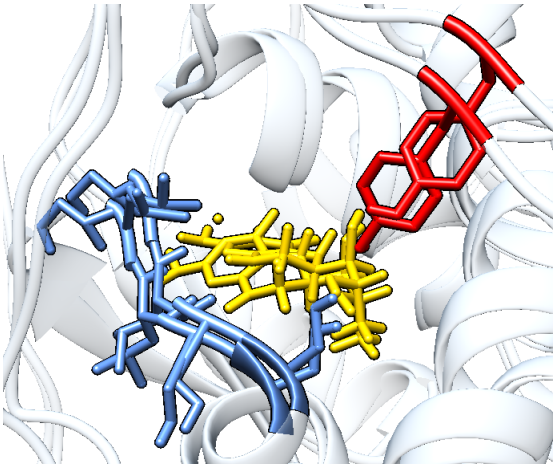

Figure 7: Overlay of structures indicative of the range of motion of the cofactor hydrogen bonding partners. Notice how much Tyr377 (in red) swings about the cofactor (in yellow) relative to the residues 147-151 (in blue).

Conclusion

In summary, QM/DMD simulations assessed whether the Solomon mechanism for the catabolism of phenylalanine by PAH could explain the sharp drop in healthy activity in the case of two disease-inducing mutants. The Solomon structure simulations capture the predicted role of both the cofactor and site of mutation on PAH activity through an dynamic, long-range pathway of communication. The results are reinforced by negative-control simulations of structures implicated in the Seigbahn mechanism and coupled-dynamics analysis. Together, they show that the orientation of BH_4 directs PAH to follow one of two pathways and is modified in the mutants by way of an interaction with Tyr377. Our discovery that a dynamic interaction correlates with PAH activity, especially in contrast to other hydrogen-bonding contacts with the cofactor that do not, demonstrates the importance of considering proteins as flexible objects comprised of an ensemble of important structures. Given the critical role of PAH and related amino acid hydroxylases in bodily amino acid regulation and their implications in disease we hope our findings and perspective will assist future biological and medical research.

Acknowledgement

The authors thank the Institute for Digital Research and Education at UCLA for supercomputer time and NSF CAREER grant NSF-CHE-1351968 for support. Professor Nikolay Dokholyan also acknowledges support from NIH grants R01GM114015, R01GM064803, and R01GM123247.

Supporting Information Available

Additional data on QM/DMD system construction, QM/DMD simulations of the Solomon system with O_2, QM/DMD convergence, and coupled-dynamic pathways of the Siegbahn system are available (PDF).

References

(1) Fitzpatrick, P. F. Tetrahydropterin-dependent amino acid hydroxylases. *Annual Review of Biochemistry* **1999**, *68*, 355–381.

(2) Kappock, T. J.; Caradonna, J. P. Pterin-dependent amino acid hydroxylases. *Chemical reviews* **1996**, *96*, 2659–2756.

(3) Kaufman, S. The phenylalanine hydroxylating system. *Advances in Enzymology and Related Areas of Molecular Biology, Volume 67* **1993**, 77–264.

(4) Mitchell, J. J.; Trakadis, Y. J.; Scriver, C. R. Phenylalanine hydroxylase deficiency. *Genetics in Medicine* **2011**, *13*, 697.

(5) Camp, K. M.; Parisi, M. A.; Acosta, P. B.; Berry, G. T.; Bilder, D. A.; Blau, N.; Bodamer, O. A.; Brosco, J. P.; Brown, C. S.; Burlina, A. B. Phenylketonuria Scientific Review Conference: state of the science and future research needs. *Molecular Genetics and Metabolism* **2014**, *112*, 87–122.

(6) Okano, Y.; Wang, T.; Eisensmith, R.; Steinmann, B.; Gitzelmann, R.; Woo, S. Missense mutations associated with RFLP haplotypes 1 and 4 of the human phenylalanine hydroxylase gene. *American journal of human genetics* **1990**, *46*, 18.

(7) Byck, S.; Tyfield, L.; Carter, K.; Scriver, C. R. Prediction of multiple hypermutable codons in the human PAH gene: codon 280 contains recurrent mutations in Quebec and other populations. *Human mutation* **1997**, *9*, 316–321.

(8) Andersen, O. A.; Flatmark, T.; Hough, E. High resolution crystal structures of the catalytic domain of human phenylalanine hydroxylase in its catalytically active Fe (II) form and binary complex with tetrahydrobiopterin1. *Journal of Molecular Biology* **2001**, *314*, 279–291.

(9) Andersen, O. A.; Flatmark, T.; Hough, E. Crystal structure of the ternary complex of the catalytic domain of human phenylalanine hydroxylase with tetrahydrobiopterin and 3-(2-thienyl)-L-alanine, and its implications for the mechanism of catalysis and substrate activation. *Journal of Molecular Biology* **2002**, *320*, 1095–1108.

(10) Lange, S. J.; Miyake, H.; Que, L. Evidence for a Nonheme Fe (IV) O Species in the Intramolecular Hydroxylation of a Phenyl Moiety. *Journal of the American Chemical Society* **1999**, *121*, 6330–6331.

(11) Panay, A. J.; Lee, M.; Krebs, C.; Bollinger Jr, J. M.; Fitzpatrick, P. F. Evidence for a high-spin Fe (IV) species in the catalytic cycle of a bacterial phenylalanine hydroxylase. *Biochemistry* **2011**, *50*, 1928–1933.

(12) Kemsley, J. N.; Wasinger, E. C.; Datta, S.; Mitić, N.; Acharya, T.; Hedman, B.; Caradonna, J. P.; Hodgson, K. O.; Solomon, E. I. Spectroscopic and Kinetic Studies of PKU- Inducing Mutants of Phenylalanine Hydroxylase: Arg158Gln and Glu280Lys. *Journal of the American Chemical Society* **2003**, *125*, 5677–5686.

(13) McKinney, J.; Teigen, K.; Frøystein, N. Å.; Salaün, C.; Knappskog, P. M.; Haavik, J.; Martínez, A. Conformation of the substrate and pterin cofactor bound to human tryptophan hydroxylase. Important role of Phe313 in substrate specificity. *Biochemistry* **2001**, *40*, 15591–15601.

(14) Fitzpatrick, P. F. Steady-state kinetic mechanism of rat tyrosine hydroxylase. *Biochemistry* **1991**, *30*, 3658–3662.

(15) Fitzpatrick, P. F. Studies of the rate-limiting step in the tyrosine hydroxylase reaction: alternate substrates, solvent isotope effects, and transition-state analogs. *Biochemistry* **1991**, *30*, 6386–6391.

(16) Chow, M. S.; Eser, B. E.; Wilson, S. A.; Hodgson, K. O.; Hedman, B.; Fitzpatrick, P. F.; Solomon, E. I. Spectroscopy and kinetics of wild-type and mutant tyrosine hydroxylase: Mechanistic insight into O2 activation. *Journal of the American Chemical Society* **2009**, *131*, 7685–7698.

(17) Bassan, A.; Blomberg, M. R.; Siegbahn, P. E. Mechanism of Dioxygen Cleavage in Tetrahydrobiopterin-Dependent Amino Acid Hydroxylases. *Chemistry - A European Journal* **2003**, *9*, 106–115.

(18) Sparta, M.; Shirvanyants, D.; Ding, F.; Dokholyan, N. V.; Alexandrova, A. N. Hybrid dynamics simulation engine for metalloproteins. *Biophysical Journal* **2012**, *103*, 767–776.

(19) Ding, F.; Tsao, D.; Nie, H.; Dokholyan, N. V. Ab initio folding of proteins with all-atom discrete molecular dynamics. *Structure* **2008**, *16*, 1010–1018.

(20) Nechay, M. R.; Gallup, N. M.; Morgenstern, A.; Smith, Q. A.; Eberhart, M. E.; Alexandrova, A. N. Histone deacetylase 8: Characterization of physiological divalent metal catalysis. *The Journal of Physical Chemistry B* **2016**, *120*, 5884–5895.

(21) Valdez, C. E.; Alexandrova, A. N. Why urease is a di-nickel enzyme whereas the CcrA β-lactamase is a di-zinc enzyme. *The Journal of Physical Chemistry B* **2012**, *116*, 10649–10656.

(22) Sparta, M.; Valdez, C. E.; Alexandrova, A. N. Metal-dependent activity of Fe and Ni acireductone dioxygenases: how two electrons reroute the catalytic pathway. *Journal of molecular biology* **2013**, *425*, 3007–3018.

(23) Valdez, C. E.; Gallup, N. M.; Alexandrova, A. N. Co2+ acireductone dioxygenase: Fe2+ mechanism, Ni2+ mechanism, or something else? *Chemical Physics Letters* **2014**, *604*, 77–82.

(24) Nedd, S.; Redler, R. L.; Proctor, E. A.; Dokholyan, N. V.; Alexandrova, A. N. Cu, Zn-superoxide dismutase without Zn is folded but catalytically inactive. *Journal of molecular biology* **2014**, *426*, 4112–4124.

(25) Morgenstern, A.; Jaszai, M.; Eberhart, M. E.; Alexandrova, A. N. Quantified electrostatic preorganization in enzymes using the geometry of the electron charge density. *Chemical Science* **2017**, *8*, 5010–5018.

(26) Valdez, C. E.; Morgenstern, A.; Eberhart, M. E.; Alexandrova, A. N. Predictive methods for computational metalloenzyme redesign–a test case with carboxypeptidase A. *Physical Chemistry Chemical Physics* **2016**, *18*, 31744–31756.

(27) Valdez, C. E.; Sparta, M.; Alexandrova, A. N. The role of the flexible L43-S54 protein loop in the CcrA metallo-β-lactamase in binding structurally dissimilar β-lactam antibiotics. *Journal of chemical theory and computation* **2012**, *9*, 730–737.

(28) Turbomole, V. 6.6; Turbomole Gmbh: Karlsruhe, Germany, 2014.

(29) Staroverov, V. N.; Scuseria, G. E.; Tao, J.; Perdew, J. P. Comparative assessment of a

new nonempirical density functional: Molecules and hydrogen-bonded complexes. *The Journal of Chemical Physics* **2003**, *119*, 12129–12137.

(30) Grimme, S.; Antony, J.; Ehrlich, S.; Krieg, H. A consistent and accurate ab initio parametrization of density functional dispersion correction (DFT-D) for the 94 elements H-Pu. *The Journal of Chemical Physics* **2010**, *132*, 154104.

(31) Weigend, F.; Ahlrichs, R. Balanced basis sets of split valence, triple zeta valence and quadruple zeta valence quality for H to Rn: Design and assessment of accuracy. *Physical Chemistry Chemical Physics* **2005**, *7*, 3297–3305.

(32) Klamt, A. Conductor-like screening model for real solvents: a new approach to the quantitative calculation of solvation phenomena. *The Journal of Physical Chemistry* **1995**, *99*, 2224–2235.

(33) Proctor, E. A.; Kota, P.; Aleksandrov, A. A.; He, L.; Riordan, J. R.; Dokholyan, N. V. Rational coupled dynamics network manipulation rescues disease-relevant mutant cystic fibrosis transmembrane conductance regulator. *Chemical Science* **2015**, *6*, 1237–1246.

(34) Dokholyan, N. V. Controlling allosteric networks in proteins. *Chemical Reviews* **2016**, *116*, 6463–6487.

Graphical TOC Entry